N76-27569

/

NASA TECHNICAL MEMORANDUM

NASA TM X-71880

NASA TM X-71880

DYNAMICS OF SOLID LUBRICATION AS OBSERVED BY OPTICAL MICROSCOPY

by Harold E. Sliney
Lewis Research Center
Cleveland, Ohio 44135

TECHNICAL PAPER to be presented at Joint Lubrication Conference
cosponsored by the American Society of Mechanical Engineers
and the American Society of Lubrication Engineers
Boston, Massachusetts, October 5-7, 1976

Prepared for ASLE/ASME

DYNAMICS OF SOLID LUBRICATION AS OBSERVED BY OPTICAL MICROSCOPY

by Harold E. Sliney

Lewis Research Center

ABSTRACT

A bench metallograph was converted into a "micro contact imager" by the addition of a tribometer employing a steel ball in sliding contact with a glass disk. The sliding contact was viewed in real time by means of projection microscope optics. The dynamics of abrasive particles and of solid lubricant particles within the contact were observed in detail. The contact was characterized by a constantly changing pattern of elastic strain with the passage of surface discontinuities and solid particles. Abrasive particles fragmented upon entering the contact, embedded in one surface and scratched the other; in contrast, the solid lubricant particles flowed plastically into thin films. The rheological behavior of the lubricating solids gave every appearance of a paste-like consistency within the Hertzian contact.

E-8653

DYNAMICS OF SOLID LUBRICATION AS OBSERVED BY OPTICAL MICROSCOPY

by Harold E. Sliney

Lewis Research Center

INTRODUCTION

Much has been written about microscopic observations of the behavior of liquid lubricants, especially in EHD contacts (e.g., refs. 1, 2). Similar observations on the dynamic behavior within unlubricated or solid lubricated contacts have been neglected. There has been no lack of analyses concerning the behavior of solid lubricants based upon crystallographic shear (ref. 3). These studies are at the atomistic level and are of fundamental importance. However, there is also much of interest and value to be learned at a larger scale characteristic of optical microscopy. Previous studies of sliding dry contacts by optical and by scanning electron microscopy have viewed the contact from the side or at an acute angle to one of the sliding surfaces (refs. 4, 5). In this manner, prow formation ahead of the sliding contact and even metallographic slip of the bearing material have been observed during sliding.

E-8653

In the present study, the entire contact was viewed directly. The sliding components were a metal ball in contact with a flat surface of a rotating glass disk. The ball was pressed against the disk to give a Hertzian contact with a circular area formed by elastic deformation of the contacting surfaces. The contact was viewed through the glass disk by a microscope in the same manner as that employed in optical interferometric studies of liquid-lubricated EHD contacts.

The scope of this study included observation of unlubricated sliding, the influence of abrasive contaminants, and lubrication with powdered molybdenum disulfide, graphite, and graphite fluoride.

APPARATUS

The ball and disk are mounted on a sliding contact machine especially designed to be fastened to a metallograph equipped with projection microscope optics. A schematic of the apparatus is shown in figure 1. The balls are 9.53 mm diameter ABEC 10 quality M-50 tool steel. The disks are optical grade borosilicate glass, 6.53 mm thick and 76.2 mm diameter. The metallograph has an inverted optical system in which the specimens are mounted above the lens system and the enlarged image of the contact is projected upon a ground glass viewing screen. The apparatus will be referred to as the "Micro Contact Imager."

A more detailed drawing of the apparatus is given in figure 2. The tribometer is rigidly and precisely mounted to the frame of the metallograph so that the microscope can be focused through the glass disk onto the Hertzian contact.

The disk drive is a variable speed DC motor with a range of 1/4 to 30 rpm. The ball is clamped in a chuck which prevents ball rotation during sliding. The ball is pneumatically loaded against the disk by regulated air pressure to a calibrated bellows. A number of different wear tracks can be obtained on one disk by translating the disk turntable relative to the ball centerline.

Procedure

The pneumatic load device was calibrated against a standardized load cell. The microscope magnification factors were obtained by calibration with an engraved slide with markings accurately spaced at 0.01 mm intervals.

When the ball is pressed against the glass disk, a circular, concentrated contact (Hertzian contact), area is formed by elastic deformation of the glass disk and to a lesser extent of the steel ball. The elastic modulus and Poisson's

ratio for glass were assumed to be 7.6×10^{10} N/m^2 (11×10^6 psi) and 0.25 respectively; those for M-50 tool steel were 2.1×10^{11} N/m^2 (30×10^6 psi) and 0.30 respectively. In figure 3, the Hertzian diameters are plotted as a function of normal load. Measured and calculated values are given. Agreement is within about 13 percent at a 4.4 N (1 lb) load and about 3.5 percent at the 13.2 N (3 lb) load, which was used in most of the experiments.

The ball and disk were solvent cleaned prior to the sliding experiments. In some experiments, the solid lubricant powder was lightly dusted onto the disk just ahead of the contact inlet; in other experiments, solid lubricant powder was intentionally trapped in the contact by loading the ball directly onto solid lubricant particles before sliding began. Photomicrographs at magnifications of 150 to 350 were taken during the sliding experiments.

RESULTS

Steel on Borosilicate Glass, Unlubricated

The concentrated contact of the M-50 tool steel ball on the glass disk can be viewed directly with the micro contact imager. Figure 4 is an example of a static contact under a load of 4.4 N (1 lb). The central, circular gray area is a Hertzian contact of 0.13 mm diameter which is formed by elastic deformation. The rings are optical interference fringes caused by the divergence of the ball away from the flat surface of the glass disk.

Dry, unlubricated sliding generally results in damage and wear to the rubbing surfaces. It is therefore of interest to observe the influence of surface features such as cracks, scratches, wear particles, and abrasive contaminants on the behavior of the contact.

Crack formation. - With a normal load applied to the ball, the contact is of course under a compressive stress component perpendicular to the direction of sliding. Additionally, it has been shown (ref. 6) that the tangential stress generated by friction creates a compressive stress component parallel to the sliding direction ahead of the contact and a corresponding tensile stress component in the wake of the contact. The location of stress reversal depends upon the friction. For a friction coefficient of 0.33, as an example, the reversal from compressive to tensile stress occurs within the contact at about one-sixth of the contact diameter from the exit and the maximum tensile stress is at the exit. The stress reversal phenomenon is an important factor in the formation and propagation of surface cracks. This was reported by others (ref. 7) and was also experimentally observed in our study.

Figure 5 shows a series of nearly identical cracks in the glass passing through the concentrated contact. In figure 5(a), a crack is barely visible at the center of the contact, where the surface is under compression. In figure 5(b), the same crack has moved near the exit where the surface is under tension and the crack has widened and has propagated laterally.

Figure 5(c) is a plot derived from reference 6 of surface stress components within the contacts and in the sliding direction. Although friction was not measured in our experiments, it is clear that crack closing under compression and widening under tension qualitatively agree with the analysis.

Influence of wear particles and abrasive contaminants. - Figure 6 shows the progress of a glass wear particle as it approaches then passes through the periphery of the Hertzian contact. The distortion of the interference fringes shows that the particle begins to redistribute the elastic strain well ahead of the contact. As the particle passes through the edge of the Hertzian

area, the contact itself is noticeably distorted.

A small amount of 400 grit (-37 micron) abrasive silicon carbide (SiC) powder was then intentionally sprinkled ahead of the contact. Figure 7(a) shows several abrasive scratches and a SiC particle which is about to enter the contact. Distortion of the interference fringes by the scratches and by the particle are apparent. Figure 7(b) shows the SiC particle, which has become embedded in the glass and has entered the contact causing a wide scratch in the tool steel and leaving a trail of very fine SiC fragments which fractured from the parent particle. Figure 7(c) shows the same particle about to leave the contact area. Figure 7(d) was recorded after only ten disc revolutions and shows the severely abraded wear scar on the ball and the pile-up of abrasive particles at the inlet region of the contact.

General observations. - These observations of a concentrated contact in unlubricated sliding show that the Hertzian area is constantly changing shape under the influence of particulates, scratches, and other surface discontinuities. Additionally, each area increment of the circular wear track on the flat surface is subjected to severe repetitive stresses.

The following sections will demonstrate that, even under lubricated conditions with good solid lubricants, there is still a surprising degree of variability in the shape of the contact as well as a remarkable mobility (flow) of the solid lubricant within the contact.

M-50 Tool Steel Ball on Borosilicate Glass - MoS_2 Lubrication

Contact initially unlubricated. - In this experiment, the unlubricated, static contact was established first. MoS_2 particles of 10 micron average size were next lightly sprinkled near the contact inlet, then sliding was begun.

This procedure was used to observe how readily MoS_2 particles would feed into the highly-stressed concentrated contact: The normal load was 13.2 N (3 lbs) which produced an average Hertzian stress of 4.1×10^8 N/m^2 (60,000 psi).

Figure 8(a) shows the first MoS_2 particles arriving at the contact inlet; the particles have penetrated the interference fringes but have not yet entered the contact. The next photograph is after 5 mm more of sliding. The MoS_2 has penetrated about 0.07 mm or one-third of the contact diameter. After an additional 10 mm of sliding, a discontinuous film of MoS_2 has extended across the entire contact diameter with some MoS_2 adhering to the glass and some to the steel ball. MoS_2 begins to pile up at the inlet to form a lubricant resevoir. In a short time, a film of MoS_2 formed over the entire length of the circular wear track on the glass disk. The film was in the form of discrete parallel streaks of lubricant alternating with some apparently unlubricated areas. No observable wear occurred during the first 200 disk revolutions. However, figure 8(d) shows that after 420 revolutions, some wear has occurred.

The ball and disk were then separated in order to more clearly observe the condition of each surface. The ball surface (fig. 8(e)) is coated with MoS_2. The underside of the wear track as viewed through the glass disk (fig. 8(f)) reveals patches of adherent MoS_2 film and little damage to the glass. The MoS_2 film was then removed from the ball contact and a flat worn area of 0.25 mm diameter can be seen in figure 8(g).

Contact initially lubricated. - Figure 9(a) shows MoS_2 powder lightly sprinkled on the disk. The next photograph shows the compaction which occurs upon contact with the ball under a static normal load of 13.5 N (3 lbs). The remaining photographs are a sequence which illustrates the ever-changing distribution of MoS_2 in the contact. The Hertzian diameter decreases

intermittently indicating that solid lubricant accumulation of the inlet can form a wedge which partially supports the load. However, after 130 disk revolutions a large increase in contact diameter indicated ball wear. Also, many scratches were evident on the glass surface.

General observations of MoS_2 lubrication. - In these experiments, there obviously was no advantage to introducing MoS_2 into the contact prior to initiating sliding. As long as MoS_2 is very near the contact inlet at the initiation of sliding, the particles are readily drawn into the converging contact and very likely are preferentially oriented crystallographically in the process.

Not only are particles readily drawn into the inlet, but MoS_2 particles are immediately deformed into very thin films of remarkable plasticity. MoS_2 within the contact flows in a manner that gives the illusion of a paste-like consistency.

M-50 Tool Steel Ball on Borosilicate Glass -
Graphite Lubrication

Contact initially unlubricated. - Figure 10 shows particles of Mexican natural graphite entering an initially-unlubricated contact and the progress of graphite through the contact. The particles enter the converging inlet region and are drawn into the Hertzian region where they lose their original identity and are smeared into a thin film in a manner similar to the behavior of MoS_2. However, graphite does not appear to adhere as effectively as MoS_2. Abrasive wear and scratches are observed after only 20 disk rotations.

Contact initially lubricated. - Figure 11(a) shows a static Hertzian zone with graphite particles trapped within the contact. The photographs that follow show that additional graphite readily enters and passes through the Hertzian contact. However, wear, especially of the glass surface, occurs rapidly.

Considerable graphite adhered to the steel ball, but much less adhered to the glass. The behavior in general was no different than in the case of graphite lubrication of the initially-unlubricated contact.

M-50 Tool Steel Ball on Borosilicate Glass - Graphite Fluoride $(CF_x)_n$ Lubrication

Figure 12 indicates the first particles of $(CF_x)_n$ entering the sliding contact, the progressive filling of the contact, and the formation of an adherent $(CF_x)_n$ film on the wear track.

The film is transparent; microscopic features on the ball surface can be observed through the film. Also the interference fringes are clearly visible on the exit side of the contact, but have slightly shifted radii caused by the finite film thickness. Track width is observable because of slight shadowing at the edges of the track; the track width is approximately equal to the contact diameter. The $(CF_x)_n$ formed a complete lubricating film in the Hertzian contact after only one-quarter revolution of the glass disk (fig. 12(d)). No measurable wear occurred until after about 100 disk rotations when the small, initial supply of lubricant was no longer adequate to maintain a complete lubricating film and a slow wear process began. The last photograph show wear on the ball and scratches on the glass after 300 disk revolutions. Abrasive wear became predominant as wear particles from the glass and the steel ball accumulated at the contact inlet.

Ball Wear

As previously indicated, the circular contact area generated when a ball is pressed against a flat surface is the result of elastic deformation. As long as the elastic limits of the specimens are not exceeded, they return to their original shape upon release of the load. However, when wear takes place

during sliding, a permanent circular wear scar is formed on the ball. Therefore during sliding, the contact area is the sum of the wear area and a peripheral area of elastic deformation.

Figure 13 shows the percentage of the total contact area which is contributed by elastic deformation, at progressive stages of ball wear. The data were experimentally obtained by periodically releasing the load and comparing the wear scar area to the area observed under load. As wear progresses, the contribution of elastic deformation rapidly decreases from 100 percent to a small percentage of the total area. Figure 13 was used as a calibration curve to correct measured contact areas during sliding for the contribution of elastic deformation. The corrected areas were converted to wear values and the results were used to obtain wear rate curves. These are summarized in figure 14.

The data of figure 14 show the very rapid wear of M-50 tool steel on unlubricated glass compared to the dramatic improvements achieved by sprinkling small amounts of solid lubricant powders on the disk. For MoS_2 and $(CF_x)_n$, there was a duration of 100 to 200 sliding cycles before measurable wear occurred. The lubricating films provided complete lubrication during this time. With continued sliding, a constant, low wear rate was measured. Graphite did not have an initial period of zero wear; ball wear began immediately at a rate about 5 times greater than the measurable wear rates with MoS_2 and graphite-fluoride lubrication.

CONCLUSIONS

The motions and deformations of unbonded lamellar solid lubricants and of abrasive particles in and around Hertzian contacts were directly observed by means of optical microscopy. These observations led to the following conclusions:

1. Solid particles readily enter the converging inlet and are subsequently drawn into the Hertzian contact itself.

2. Solid lubricant particles, upon entering the Hertzian region are immediately compressed and sheared into very thin films. This deformation involves severe plastic flow which gives a paste-like appearance to the rheological behavior of the lubricants within the contact.

3. Adjacent lubricant particles immediately coalesce upon entering the contact and flow together into a thin film in which the original boundaries between particles are no longer distinguishable.

4. MoS_2 and $(CF_x)_n$ flowed more readily than graphite and tended to form more continuous films in the contact. This appears to correlate with the lower wear rates obtained with MoS_2 and $(CF_x)_n$ lubrication.

5. If the arrival rate of lubricant particles at the contact is adequate, excess particles accumulate at the inlet where they act as a resevoir from which lubricant is fed into the contact. When the arrival rate is too low, the existing film wears and unlubricated contacts ensue.

6. In unlubricated sliding, cracks rapidly form in the glass. The cracks are perpendicular to the sliding direction and form within the contact in the region where the stresses parallel to the surface reverse from compression to tension.

7. Hard particles and surface imperfections such as scratches cause highly localized, severe distortions of the contact geometry.

8. The principle observable difference in the dynamics of solid lubricant particles and abrasive particles in a contact is that lubricating solids undergo severe plastic flow, while abrasives do not. The lubricants plastically flow to form films which separate the sliding surface. While the abrasive particles embed in one surface and abrade the other.

REFERENCES

1. Foord, C. A., Hammann, W. C., and Cameron, A., Evaluation of Lubricants Using Optical Elastohydrodynamics, ASLE Transactions 11, 31-43 (1968).

2. Wedeven, L. D., Traction and Film Thickness Measurements Under Stained Elastohydrodynamic Conditions, Jour. of Lubr. Technology, 97, series F, no. 2, 321-329 (1975).

3. Buckley, D. H., Friction Wear and Lubrication in Vacuum, NASA SP-277, 1971.

4. Stuber, C. D., A Microscopic Study of the Friction Process. PhD Thesis, Ohio State University, Columbus, 1968.

5. Brainard, W. A., and Buckley, D. H., Dynamic Scanning Electron - Microscope Study of Friction and Wear. NASA TN D-7700, June 1974.

6. Seely, F. B., and Smith, J. O., Advanced Mechanics of Materials, John Wiley & Sons Inc., N. Y., 1952.

7. Bowden, F. P. and Tabor, D., The Friction and Lubrication of Solids, II, Oxford at the Clavendon Press, 1964, pp. 19-20.

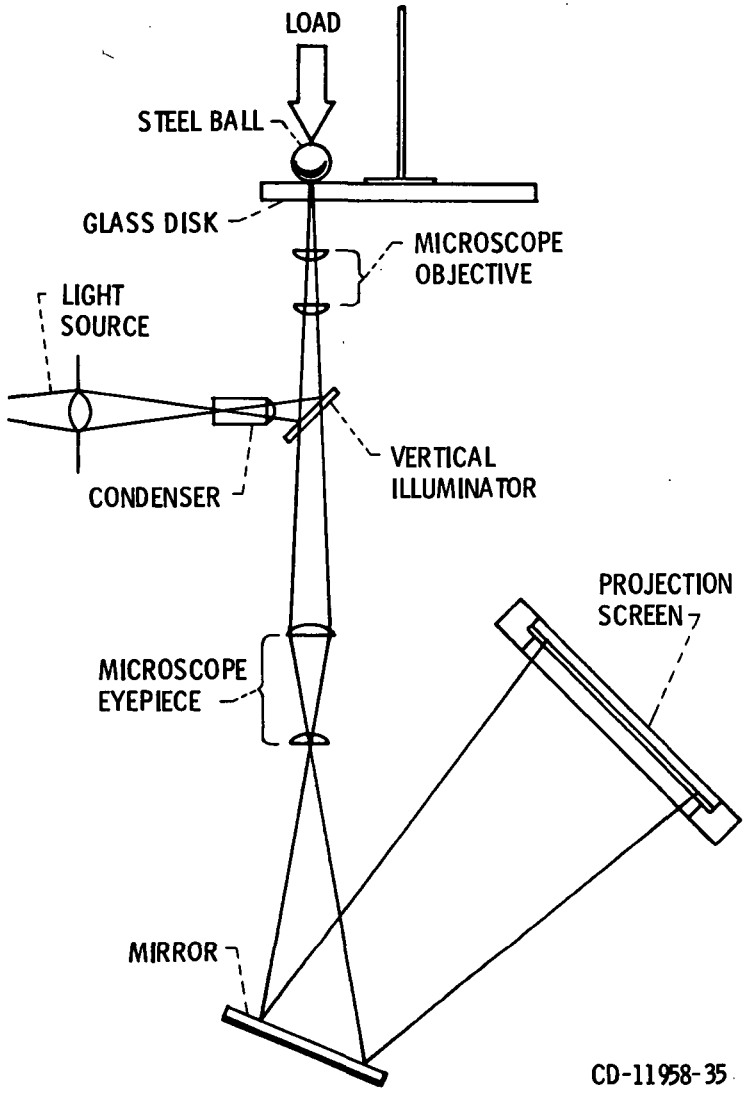

Figure 1. - Schematic of optical system.

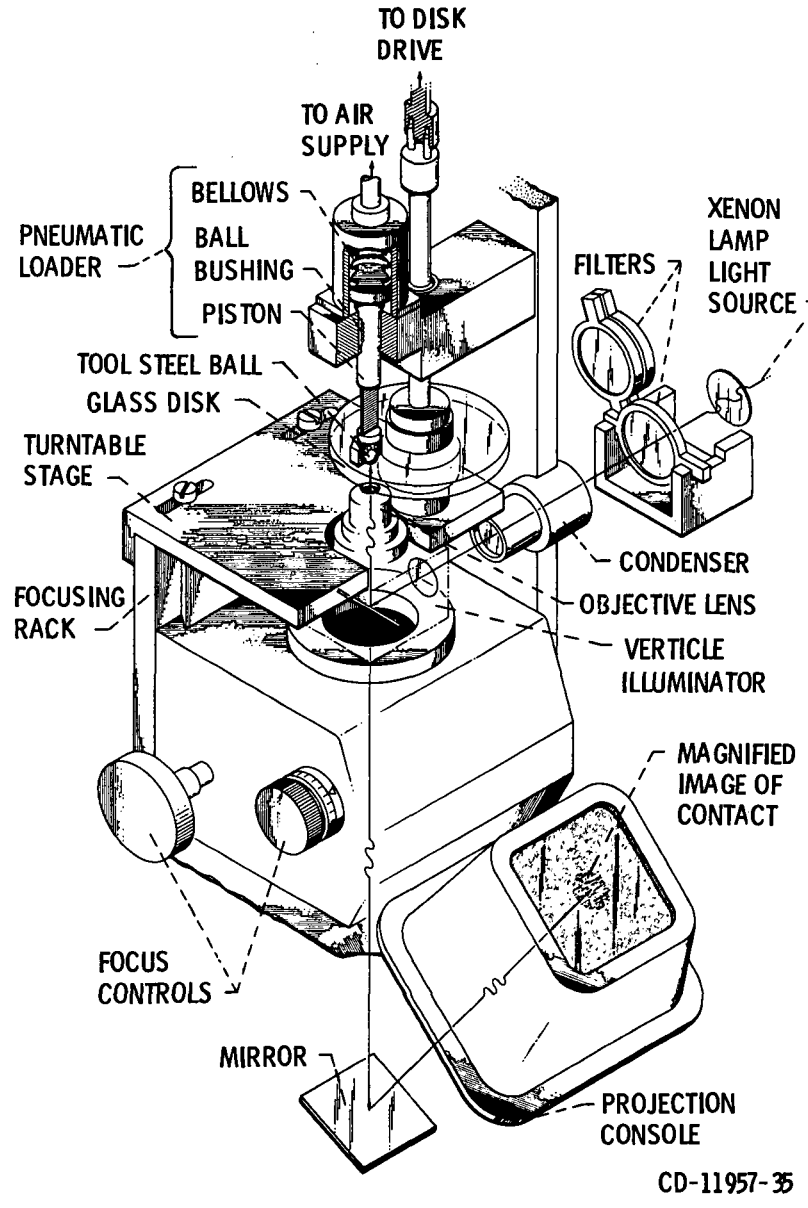

Figure 2. - Micro contact imager.

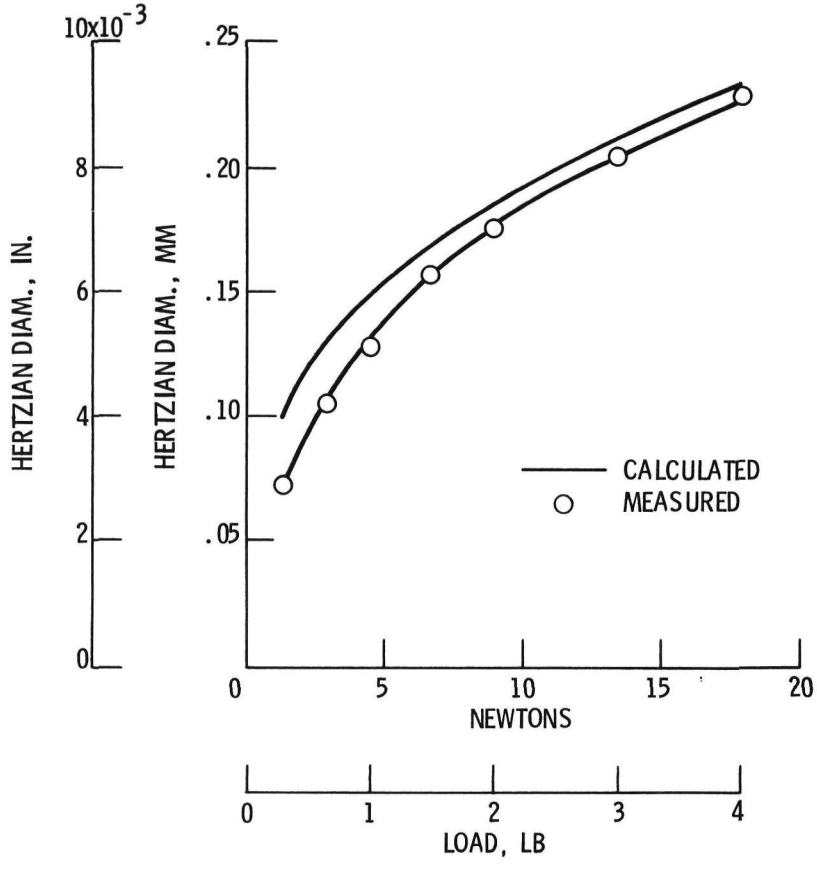

Figure 3. - Diameter of Hertzian contact area generated by an M-50 tool steel ball pressed against a flat borosilicate glass disk, all, diam., 9.5 mm, (0.375 in.).

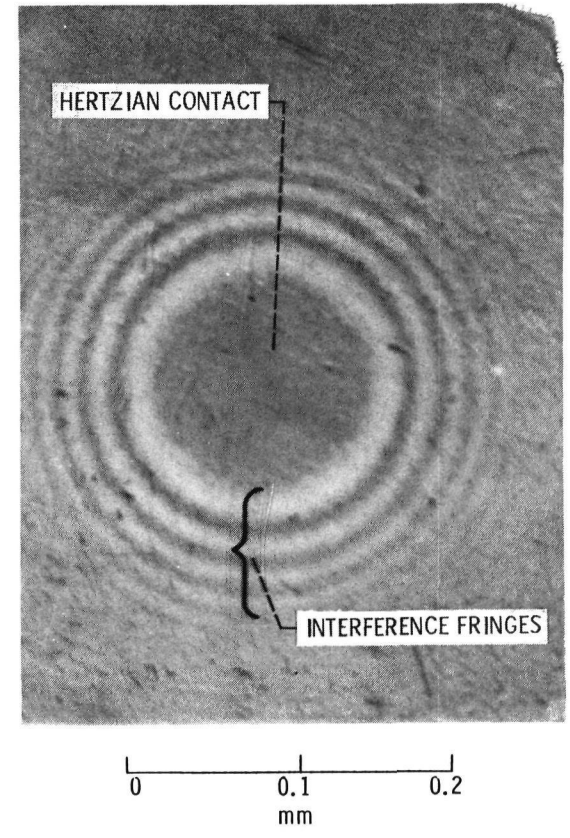

Figure 4. - Static contact 4.4 N (1 lb) load. Central circle is contact area formed by elastic deformation at contact of tool steel ball on a glass flat. Original magnification, X250.

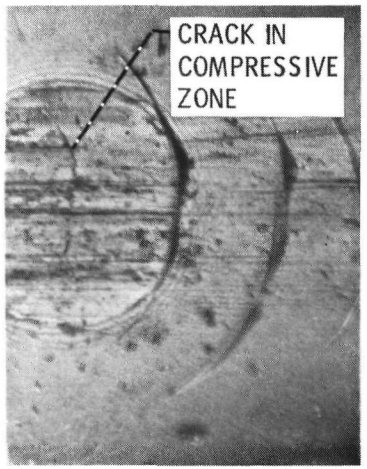

(a) CRACK IN COMPRESSION.

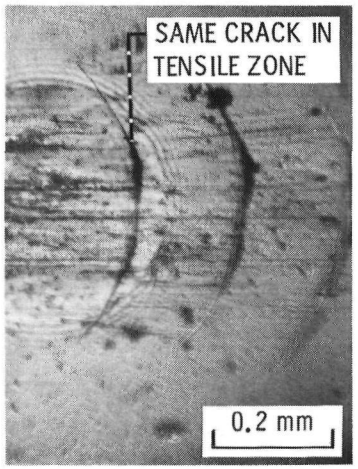

(b) CRACK IN TENSION.

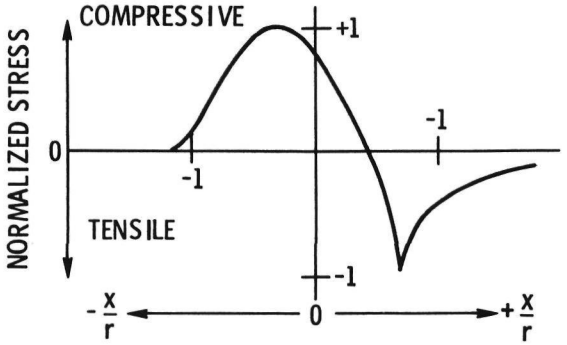

LOCATION RELATIVE TO HERTZIAN RADIUS, r

SLIDING DIRECTION OF GLASS ➞

(c) SURFACE STRESS COMPONENT IN SLIDING DIRECTION.

Figure 5. - Crack formation and propagation in unlubricated contact. Load, 13.2 N (3 lb); original magnification, X150.

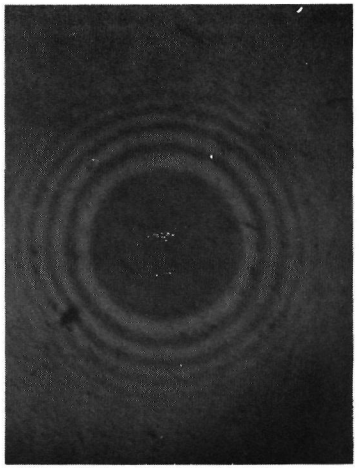

(a) PARTICLE AT INLET.

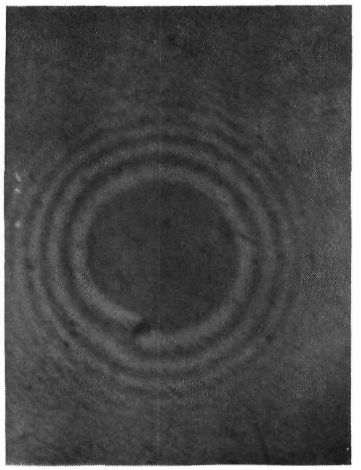

(b) PARTICLE IN THE CONTACT.

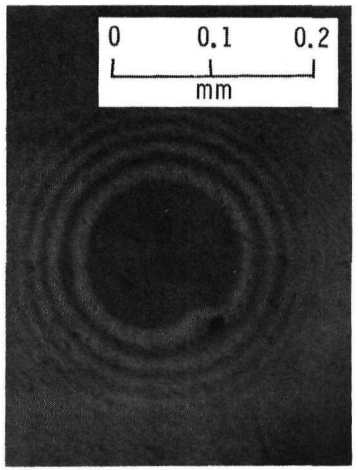

(c) PARTICLE EXITING THE CONTACT.

SLIDING DIRECTION OF GLASS ➞

Figure 6. - Passage of a glass wear particle through the periphery of a concentrated contact. Load, 4.4 N (1 lb); original magnification, X250.

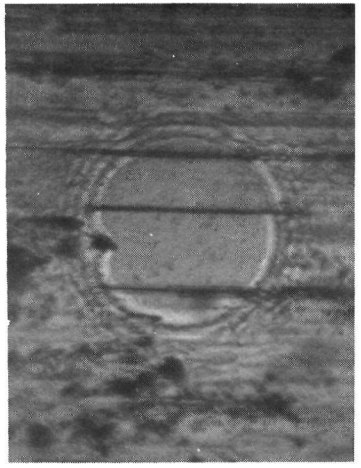

(a) SiC PARTICLE ENTERING CONTACT.

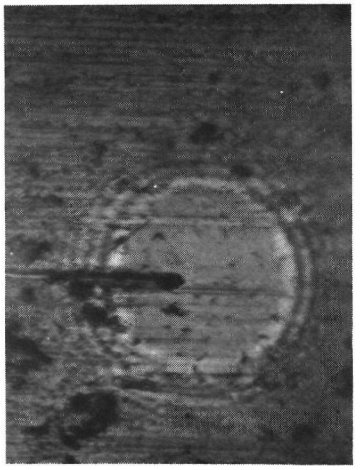

(b) PARTICLE PART WAY THROUGH CONTACT.

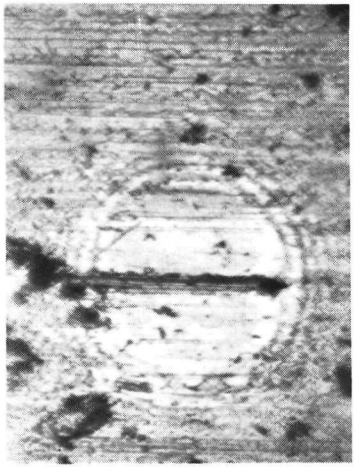

(c) PARTICLE AT CONTACT EXIT.

(d) CONTACT AFTER 10 DISK REVOLUTIONS.

Figure 7. - Abrasive action of silicon carbide particles. Load, 13.2 N (3 lb); original magnification, X150.

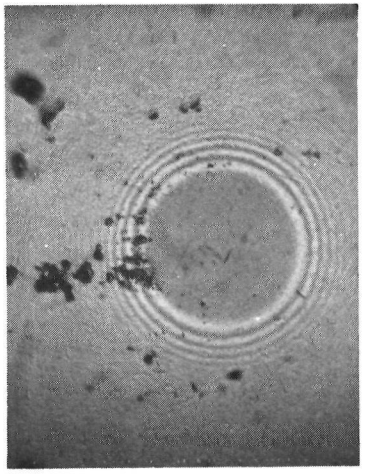

(a) LUBRICANT PARTICLES APPROACHING CONTACT.

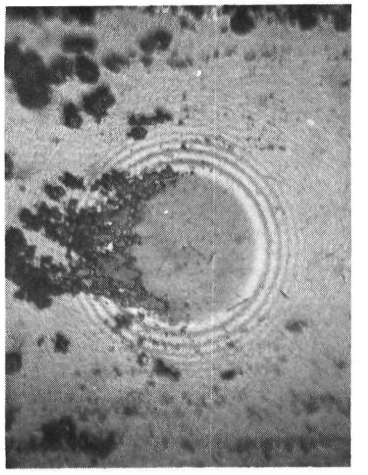

(b) PARTICLES ENTERING CONTACT.

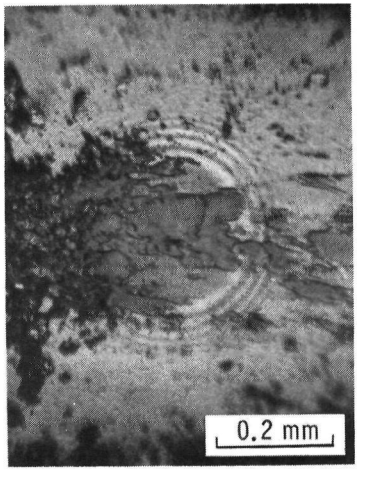

(c) EXTENSIVE PLASTIC FLOW OF MoS_2 IN CONTACT.

Figure 8. - Behavior of MoS_2 powder in an initially unlubricated contact, 13.2 N (3 lb) load. Original magnification, X150.

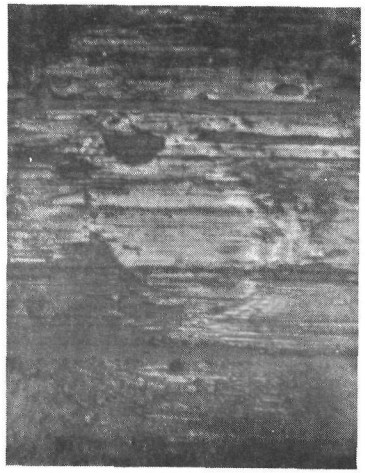

(d) BALL/DISK CONTACT.

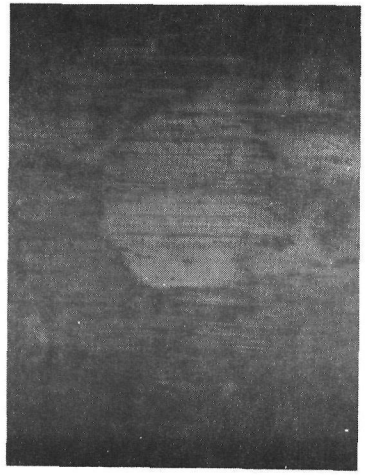

(e) BALL CONTACT (NOTE COMPLETE MoS_2 FILM).

(f) UNDERSIDE OF DISK WEAR TRACK.

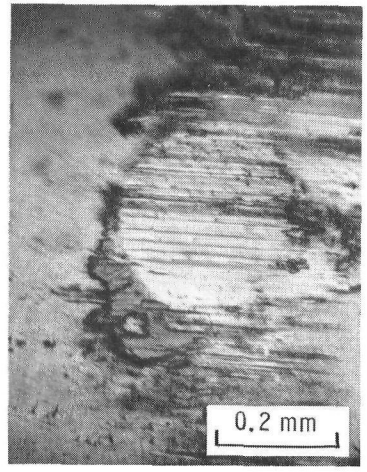

(g) BALL WEAR SCAR WITH FILM REMOVED BUT WITH COMPACTED MoS_2 STILL AT INLET.

Figure 8. - Concluded. Contact after 420 disk revolutions.

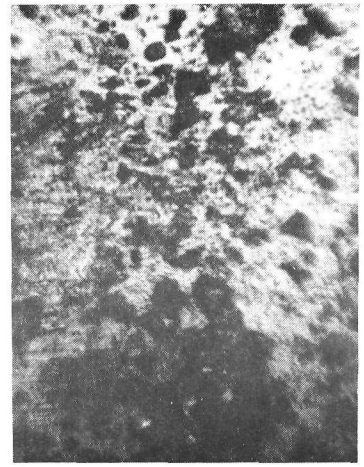

(a) LOOSE MoS_2 POWDER ON GLASS DISK.

(b) MoS_2 IN STATIC CONTACT (13.2 N).

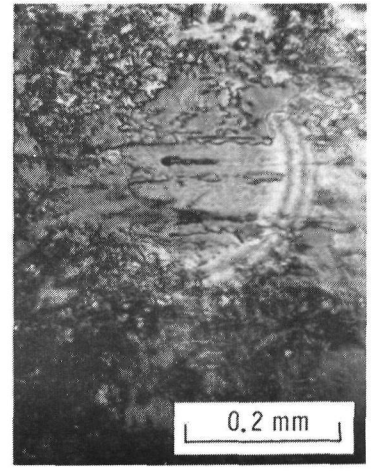

SLIDING DIRECTION OF GLASS →

(c) CONTACT AT INITIATION OF SLIDING.

Figure 9. - Behavior of MoS_2 in an initial static contact followed by sliding contact, 13.2 N (3 lb) load; original magnification, X200.

(d)

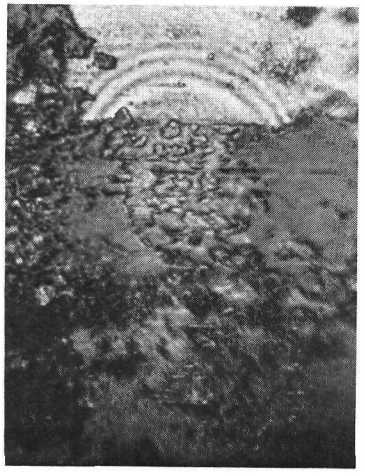

(e)

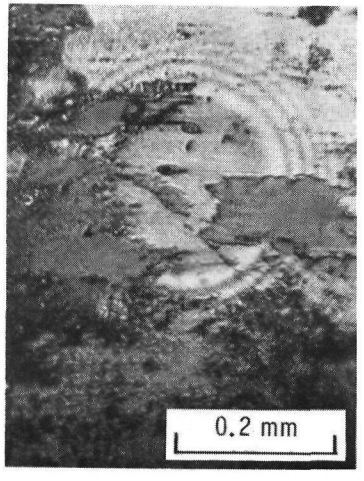

(f)

Figure 9. - Concluded. Changing pattern of MoS_2 distribution during sliding.

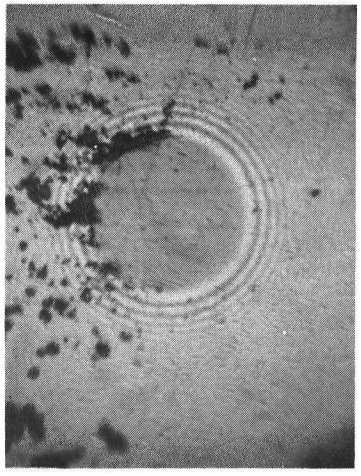

(a) PARTICLES ENTERING CONTACT.

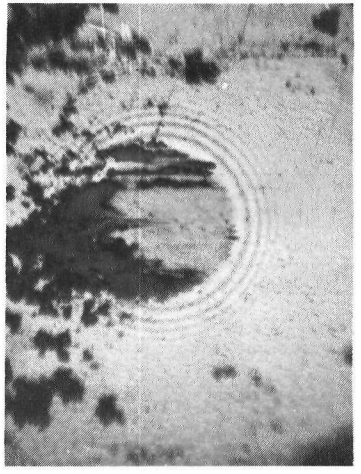

(b) PASSAGE OF GRAPHITE THROUGH CONTACT.

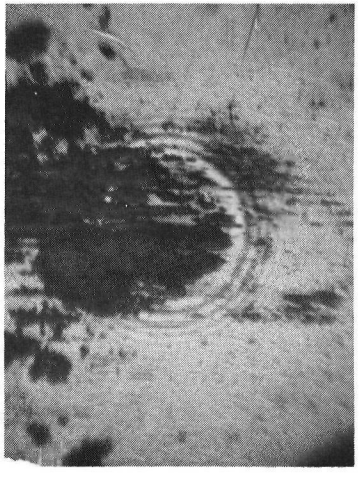

(c) PASSAGE OF GRAPHITE THROUGH CONTACT.

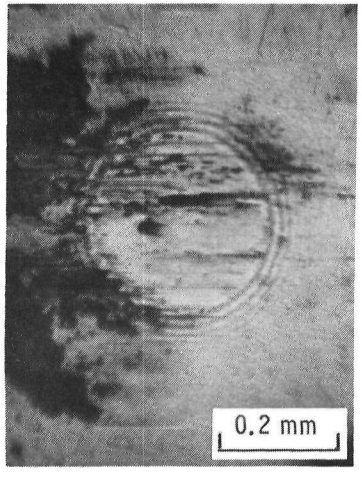

(d) CONTACT AFTER 20 DISK REVOLUTIONS.

Figure 10. - Behavior of Mexican graphite in an initially unlubricated contact; load, 13.2 N (3 lb); original magnification, X150.

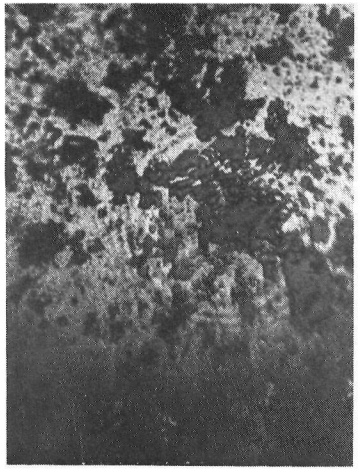

(a) GRAPHITE IN STATIC CONTACT (13.2 N LOAD).

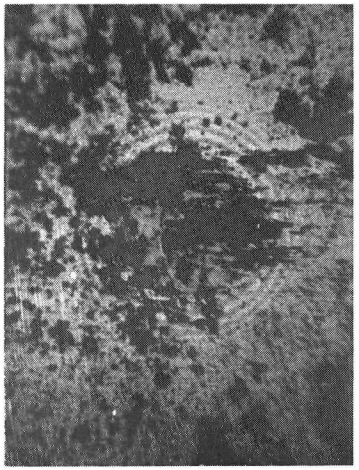

(b) CONTACT AS SLIDING BEGINS.

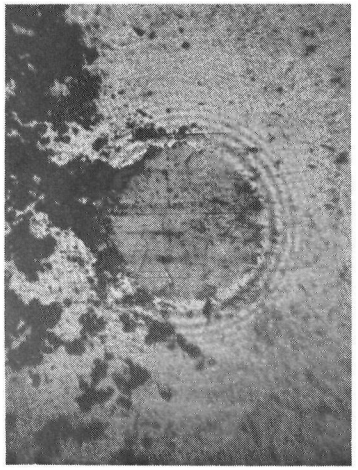

(c) CONTACT AFTER 1/4 DISK REVOLUTION.

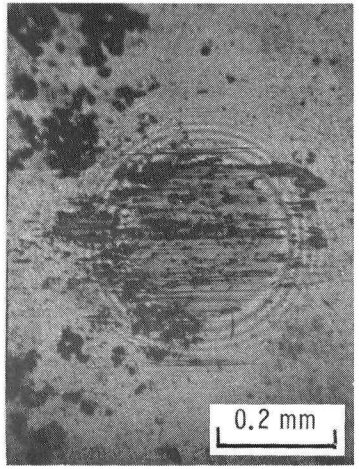

(d) CONTACT AFTER 2 DISK REVOLUTIONS.

Figure 11. - Behavior of natural (Mexican) graphite in an initial static contact followed by sliding contact; original magnification, X150.

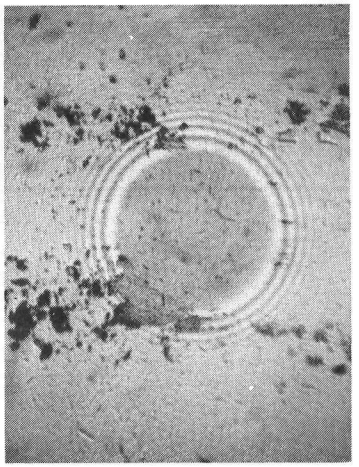

(a) FIRST PARTICLES ENTERING CONTACT.

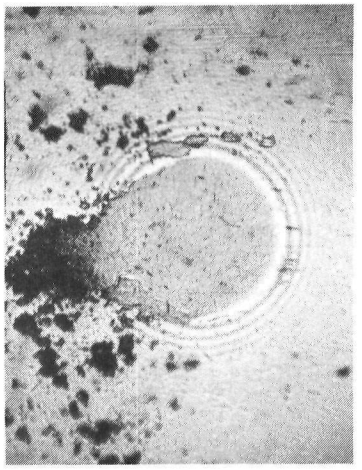

(b) PROGRESSIVE FILM FORMATION.

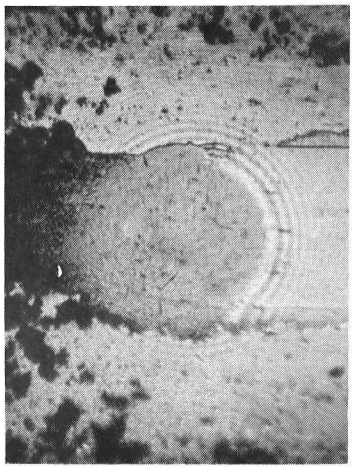

(c) PROGRESSIVE FILM FORMATION.

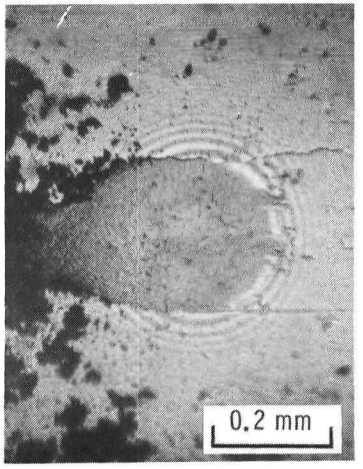

(d) COMPLETE FILM FORMATION AFTER ONLY 10 mm OF SLIDING.

Figure 12. - Behavior of graphite fluoride in initially unlubricated contact. Load, 13.2 N (3 lb); original magnification, X150.

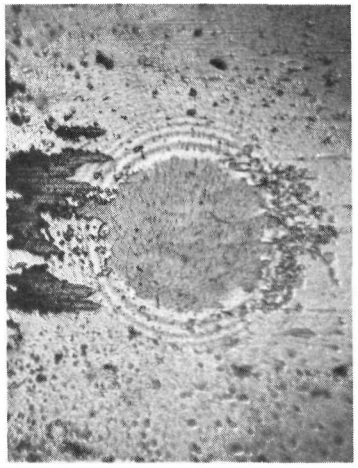

(e) CONTACT AFTER 1/4 REVOLUTION (40 mm OF SLIDING.

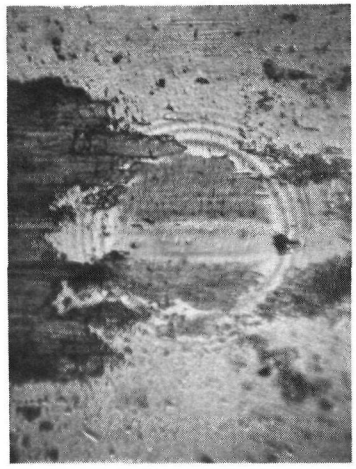

(f) CONTACT AFTER 20 REVOLUTIONS.

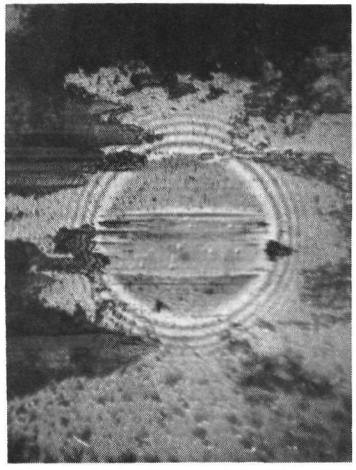

(g) CONTACT AFTER 40 REVOLUTIONS.

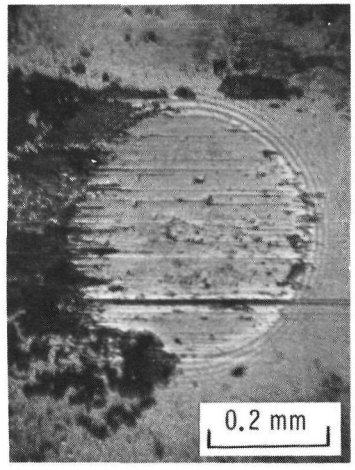

(h) CONTACT AFTER 300 REVOLUTIONS.

Figure 12. - Concluded.

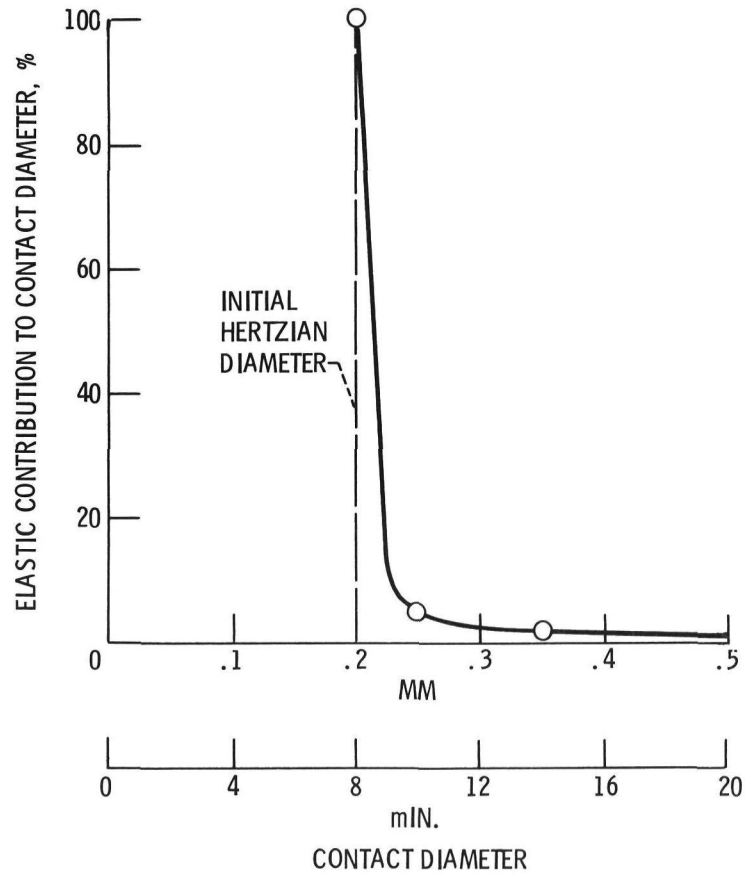

Figure 13. - Calibration curve to correct wear circle diameter for elastic deformation, tool steel ball, 9.5 mm (0.375 in.) diam., glass disk, 13.2 N (3 lb) load.

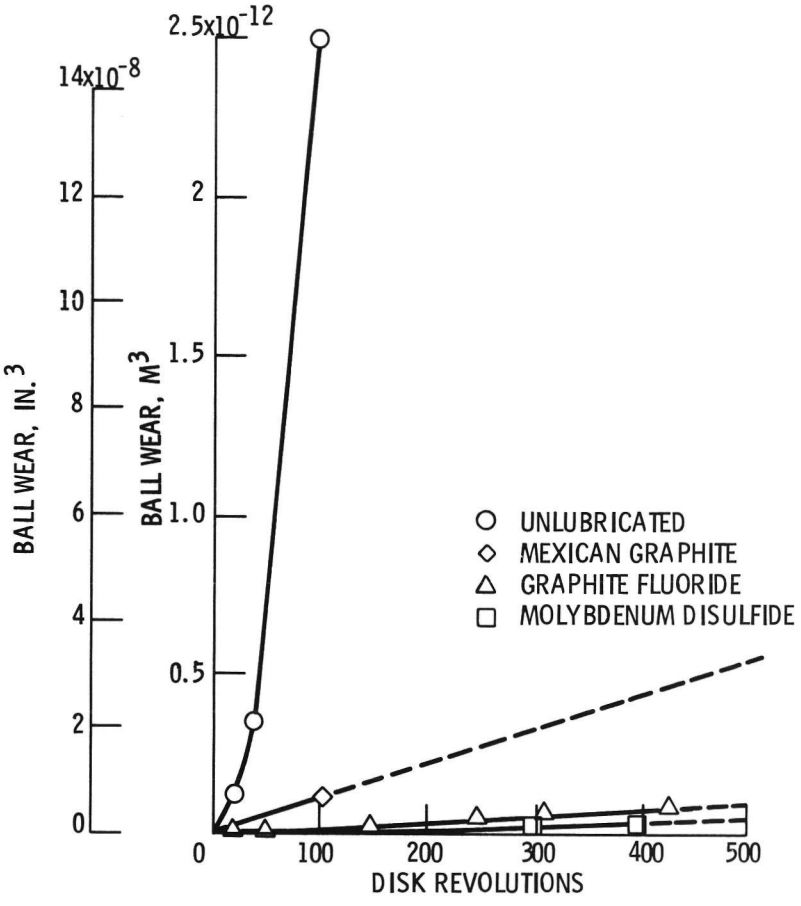

Figure 14. - Wear of ball sliding on glass: unlubricated and lubricated. Ball, 9.5 mm (0.375 in.) diam., 13.2 N (3 lb) load.